

## Magnetic biodegradable Fe<sub>3</sub>O<sub>4</sub>/CS/PVA nanofibrous membranes for bone regeneration

This article has been downloaded from IOPscience. Please scroll down to see the full text article.

2011 Biomed. Mater. 6 055008

(<http://iopscience.iop.org/1748-605X/6/5/055008>)

View [the table of contents for this issue](#), or go to the [journal homepage](#) for more

Download details:

IP Address: 222.28.99.62

The article was downloaded on 06/09/2011 at 10:03

Please note that [terms and conditions apply](#).

# Magnetic biodegradable Fe<sub>3</sub>O<sub>4</sub>/CS/PVA nanofibrous membranes for bone regeneration

Yan Wei<sup>1,4</sup>, Xuehui Zhang<sup>1</sup>, Yu Song<sup>2</sup>, Bing Han<sup>3</sup>, Xiaoyang Hu<sup>1</sup>,  
Xinzhi Wang<sup>4</sup>, Yuanhua Lin<sup>2</sup> and Xuliang Deng<sup>1,4,5</sup>

<sup>1</sup> Department of Geriatric Dentistry, School and Hospital of Stomatology, Peking University, Beijing, 100081, People's Republic of China

<sup>2</sup> State Key Laboratory of New Ceramics and Fine Processing, Department of Materials Science and Engineering, Tsinghua University, Beijing, 100084, People's Republic of China

<sup>3</sup> Department of Orthodontics, School and Hospital of Stomatology, Peking University, Beijing, 100081, People's Republic of China

<sup>4</sup> Department of Prosthodontics, School and Hospital of Stomatology, Peking University, Beijing, 100081, People's Republic of China

E-mail: [kqdengxuliang@bjmu.edu.cn](mailto:kqdengxuliang@bjmu.edu.cn)

Received 12 May 2011

Accepted for publication 8 August 2011

Published 5 September 2011

Online at [stacks.iop.org/BMM/6/055008](http://stacks.iop.org/BMM/6/055008)

## Abstract

In recent years, interest in magnetic biomimetic scaffolds for tissue engineering has increased considerably. The aim of this study is to develop magnetic biodegradable fibrous materials with potential use in bone regeneration. Magnetic biodegradable Fe<sub>3</sub>O<sub>4</sub>/chitosan (CS)/poly vinyl alcohol (PVA) nanofibrous membranes were achieved by electrospinning with average fiber diameters ranging from 230 to 380 nm and porosity of 83.9–85.1%. The influences of polymer concentration, applied voltage and Fe<sub>3</sub>O<sub>4</sub> nanoparticles loading on the fabrication of nanofibers were investigated. The polymer concentration of 4.5 wt%, applied voltage of 20 kV and Fe<sub>3</sub>O<sub>4</sub> nanoparticles loading of lower than 5 wt% could produce homogeneous, smooth and continuous Fe<sub>3</sub>O<sub>4</sub>/CS/PVA nanofibrous membranes. X-ray diffraction (XRD) data confirmed that the crystalline structure of the Fe<sub>3</sub>O<sub>4</sub>, CS and PVA were maintained during electrospinning process. Fourier transform infrared spectroscopy (FT-IR) demonstrated that the Fe<sub>3</sub>O<sub>4</sub> loading up to 5 wt% did not change the functional groups of CS/PVA greatly. Transmission electron microscopy (TEM) showed islets of Fe<sub>3</sub>O<sub>4</sub> nanoparticles evenly distributed in the fibers. Weak ferrimagnetic behaviors of membranes were revealed by vibrating sample magnetometer (VSM) test. Tensile test exhibited Young's modulus of membranes that were gradually enhanced with the increase of Fe<sub>3</sub>O<sub>4</sub> nanoparticles loading, while ultimate tensile stress and ultimate strain were slightly reduced by Fe<sub>3</sub>O<sub>4</sub> nanoparticles loading of 5%. Additionally, MG63 human osteoblast-like cells were seeded on the magnetic nanofibrous membranes to evaluate their bone biocompatibility. Cell growth dynamics according to MTT assay and scanning electron microscopy (SEM) observation exhibited good cell adhesion and proliferation, suggesting that this magnetic biodegradable Fe<sub>3</sub>O<sub>4</sub>/CS/PVA nanofibrous membranes can be one of promising biomaterials for facilitation of osteogenesis.

(Some figures in this article are in colour only in the electronic version)

<sup>5</sup> Author to whom any correspondence should be addressed.

## 1. Introduction

Scaffolds play a pivotal role in tissue regeneration, which provides specific macro and micro structure to modify the biological and biomechanical reaction of the cells during the healing process [1, 2]. Especially when the scaffolds are implanted in the bodies to help rebuild damaged or diseased tissues, it is essentially important to regulate the cell adhesion, proliferation, and metabolism through the characteristics of scaffolds, which has become a research focus in the area of tissue regeneration [3, 4].

Magnetic nanoparticles are of great interest owing to their potential biomedical applications [5–9], such as cell expansion, cell sheets construction, magnetic cell seeding, drug delivery vehicle and cancer hyperthermia treatment, due to their unique feature of orientational movement in magnetic field. Recently, several pieces of research have demonstrated that magnetic nanoparticles have effect of osteoinduction even without external magnetic force. Gu *et al* [10] reported that the introduction of magnetic nanoparticles to CaP bioceramics could promote bone formation and growth *in vitro* and *in vivo*. Meng *et al* [11] demonstrated that the addition of magnetic nanoparticles in hydroxyapatite nanoparticles (nHA)/poly (D, L-lactide) (PLA) composite nanofibrous films could induce a significantly higher proliferation rate and faster differentiation of osteoblast cells. Therefore, scaffolds containing magnetic nanoparticle may provide great potential in bone regenerative medicine.

Electrospinning is a versatile process of fabricating nanofibers. Electrospun nanofibrous membranes are considered to be of great potential in the field of tissue regeneration, since they can closely mimic the extracellular matrix architecture [12–16]. The electrospinning process also provides operational flexibility for incorporating multiple components into nanofiber, such as metal nanoparticles (Pt, Ag, Au) [17–19] and inorganic compound nanoparticles ( $\text{TiO}_2$ ,  $\text{SiO}_2$ ) [20, 21]. As well, electrospinning technique had been successfully used in fabricating magnetic fibrous scaffolds ( $\text{Fe}_3\text{O}_4$ /PVA nanofibers [22],  $\text{Fe}_3\text{O}_4$ /PVP nanofibers [23],  $\text{Fe}_3\text{O}_4$ /C nanofibers [24],  $\text{Fe}_3\text{O}_4$ /CECh/PAA [25], FePt/PCL nanofibers [26],  $\text{CoFe}_2\text{O}_4$ /PAN nanofibers and  $\text{CoFe}_2\text{O}_4$ /carbon nanofibers [27]). However, in these studies, the cell function and the potential use of magnetic fibrous scaffolds in tissue engineering have not been clearly clarified.

Chitosan (CS), similar to glycosaminoglycans (GSGs, which is an important copolymer in extracellular matrix), is the only native polysaccharide ever found by now with alkalinescence and positive charge. It has been widely investigated because of its excellent biocompatibility, appropriate biodegradability, excellent antibacterial property and capability of promoting proliferation of osteoblasts [28–31]. It is hard to electrospin fibers from aqueous solutions of pure CS, due to the high viscosity and chain entanglement of CS [28, 29]. Poly vinyl alcohol (PVA), which has drawn much attention because of its water-solubility, chemical stability, biocompatibility, inherent fiber- and film-forming ability, is proposed to decrease the high

viscosity and chain entanglement of CS, and consequently facilitate easy electrospinning [29, 30]. Electrospun CS/PVA nanofibrous membranes were considered to have not only the osteoconductivity of CS but also good electrospinnability and mechanical properties, which make it a possible candidate material for use in tissue engineering applications [32–34]. However, the preparation of magnetic CS/PVA nanofibrous membranes has not yet been reported. Whether the incorporation of magnetic materials could promote the application of CS/PVA nanofibrous membranes in the area of tissue regeneration is still unclear.

In this work, magnetic biodegradable  $\text{Fe}_3\text{O}_4$ /CS/PVA nanofibrous membranes were successfully fabricated by the electrospinning process. The influences of polymer concentration, applied voltage and  $\text{Fe}_3\text{O}_4$  nanoparticles loading on the formation of magnetic nanofibers were investigated in detail. In order to explore the potential application of the magnetic  $\text{Fe}_3\text{O}_4$ /CS/PVA nanofibrous membranes in bone regeneration, the MG63 human osteoblast-like cells were seeded on the magnetic nanofibrous membranes, and their adhesion and proliferation were examined to inspect the cell growth dynamics.

## 2. Materials and methods

### 2.1. Materials

Reagents used in this study included the following:  $\text{FeCl}_3 \cdot 6\text{H}_2\text{O}$  and  $\text{FeCl}_2 \cdot 4\text{H}_2\text{O}$  (Sinopharm Chemical Reagent Co., Ltd, China), sodiumcitrate (Aladdin Co., Ltd, China), chitosan (CS,  $M_v = 6 \times 10^5$ , with  $88.33 \pm 1.11\%$  deacetylation degree, Aladdin Co., Ltd, China), polyvinyl alcohol (PVA,  $M_n = 4.9 \times 10^4$ , degree of hydrolysis: 86–89%, Aladdin Co., Ltd, China), human osteoblast-like cells (MG-63) were obtained from the American Type Cell Culture Collection (ATCC, Rockville, MD, USA). Dulbecco's modified Eagle's medium (DMEM, Gibco, USA), fetal bovine serum (FBS, Gibco, USA), penicillin (Gibco, USA), streptomycin (Gibco, USA), trypsinase (Sigma, USA).

### 2.2. Fabrication of $\text{Fe}_3\text{O}_4$ /CS/PVA nanofibrous membranes by electrospinning process

$\text{Fe}_3\text{O}_4$  nanoparticles were obtained by a co-precipitation method and modified with sodiumcitrate as our previous work [35]. CS and PVA were individually dissolved in acetic acid and deionized water at a concentration of 2% wt, then these two solutions were mixed at the weight ratio of CS/PVA = 2:3,  $\text{Fe}_3\text{O}_4$  nanoparticles and ethanol alcohol were added into the mixture. This polymer solution was constantly and controllably supplied using a syringe pump (NE-300, New Era Pump Systems, Inc.) to 5 ml syringe equipped with a 0.60 mm (inner diameter) stainless steel gauge needle. The needle was connected to a high voltage power supply (Gamma High Voltage Research, Product HV power Supply, Model No ES3UP-5w/DAM) with a dc voltage up to 30 kV. The feed rate was fixed at  $0.3 \text{ ml h}^{-1}$  and the distance from the conical nozzle to the collector was controlled at 10 cm. The grounded counter electrode was a flat aluminum foil. The electrospun

nanofiber was collected on the aluminum foil and accumulated to a thin membrane. All the obtained fibrous membranes were dried in vacuum to remove solvent residues

To investigate the influence of electrospinning parameters on the formation of magnetic nanofibers, four kinds of polymer concentration (3.5, 4.0, 4.5 and 5.0 wt%), four types of applied voltage (10, 15, 20, and 25 kV) and three Fe<sub>3</sub>O<sub>4</sub> nanoparticles loading (1, 3 and 5 wt%) were selected.

### 2.3. Electrospun Fe<sub>3</sub>O<sub>4</sub>/CS/PVA nanofibrous membranes morphology observation

The morphologies of electrospun nanofibrous membranes were observed under field-emission scanning electron microscopy (FESEM, Hitachi S-4700 FEG) after gold sputter-coating. The average nanofiber diameters were determined by measuring 100 individual nanofibers from FESEM images using ImageJ software (National Institutes of Health). Transmission electron microscopy (TEM, Hitachi H-600-II, Japan) was used to determine the distribution of Fe<sub>3</sub>O<sub>4</sub> nanoparticles inside the nanofibrous membranes.

### 2.4. Porosity and apparent density measurement of electrospun Fe<sub>3</sub>O<sub>4</sub>/CS/PVA nanofibrous membranes

Membranes were maintained in distilled water for three minutes, then they were weighed after mopping superficial water with filter paper. The wet membrane was placed in a freezer dryer for 72 h before measuring the dry weight. The porosity of membrane was calculated using equation as  $P(\%) = (Q_0 - Q_1)/Ah$  and the apparent density was calculated using equation as  $\rho = Q_1/Ah$ , where  $P$  is the porosity of membrane,  $\rho$  the apparent density,  $Q_0$  the wet sample weight (g),  $Q_1$  the dry sample weight (g),  $A$  the square of membrane (cm<sup>2</sup>) and  $h$  is the thickness of membrane ( $\mu$ m). In order to minimize experimental error, each membrane was measured for three times and calculated average [36].

### 2.5. XRD analysis

XRD patterns of the Fe<sub>3</sub>O<sub>4</sub>/CS/PVA membranes were examined to study the crystalline structure and compared them with those of pure Fe<sub>3</sub>O<sub>4</sub> and CS/PVA electrospun membranes.

### 2.6. Vibrating sample magnetometer examination

Magnetic properties of the Fe<sub>3</sub>O<sub>4</sub>/CS/PVA membranes were measured using a vibrating sample magnetometer (VSM, LakeShore 7307).

### 2.7. FTIR spectroscopy

Fourier transform infrared spectroscopy (FTIR) studies were carried out on compressed films containing KBr pellets and samples using a FTIR spectrophotometer (Nicolet8700, USA). All spectra were recorded in absorption mode at 2 cm<sup>-1</sup> intervals and in the wavelength range 3800–400 cm<sup>-1</sup>.

### 2.8. Tensile test

The magnetic Fe<sub>3</sub>O<sub>4</sub>/CS/PVA nanofibrous membranes were carefully cut into rectangles (0.04 × 5 × 20 mm<sup>3</sup>) and a tensile test was conducted by an Instron (Model 1221, USA) at a 20 mm min<sup>-1</sup> crosshead speed at room temperature. The tensile stress of each membrane was calculated from the nominal cross-sectional area of the tensile specimen.

### 2.9. Cell seeding and morphology observation

After sterilization using <sup>60</sup>Co with a total dose of 25 kGy, the Fe<sub>3</sub>O<sub>4</sub>/CS/PVA nanofibrous membranes were cut into circular discs to fully cover the bottom of 24-well tissue culture plates. MG63 human osteoblast-like cells were seeded at a density of 1 × 10<sup>4</sup> cells/well. The plates were maintained in a humidified atmosphere with 5% CO<sub>2</sub> at 37 °C and cultured in DMEM supplemented with 10% FBS, which was changed every 2–3 days.

At experimental days of 1, 3 and 7, the supernatants were removed and the membrane surfaces were washed twice with PBS. The cells were fixed with 2.5% glutaraldehyde in PBS overnight at 4 °C. After being washed with PBS, the specimens were dehydrated using diluted series of ethanol concentration (20, 50, 70 and 90%) for 10 min, and then dehydrated twice with 100% ethanol for 10 min. After critical point drying, specimens were gold sputter-coated in a vacuum and cell adhesion and proliferation were examined by SEM.

### 2.10. MTT assay

The numbers of viable cells the Fe<sub>3</sub>O<sub>4</sub>/CS/PVA membranes were measured by a MTT assay. The mechanism of the MTT assay is that metabolically active cells react with a tetrazolium salt in the MTT agent to produce a soluble formazan dye which can be absorbed at a wavelength of 490 nm [37]. The assay was performed by enzyme immunoassay kits (KHB ST-360, Shanghai Kehua Bio-engineering Co., Ltd. China) after 1, 3, 5 and 7 days, and the values were compared to understand the difference in cell adhesion and proliferation on nanofibers. TCPs (tissue culture plates) were used as control.

### 2.11. Statistical analysis

Statistical analysis was performed using an SPSS 10 statistical package and values were considered significant at  $p < 0.05$ . One-way analysis of variance (ANOVA) and Student–Newman–Keuls (S–N–K) test were used for multiple comparisons of different groups.

## 3. Results

### 3.1. Morphology observation of Fe<sub>3</sub>O<sub>4</sub>/CS/PVA nanofibrous membranes

Homogeneous and smooth surface were achieved only from solutions with the polymer concentration of 4.5 wt% (figures 1(c1) and (c2)) and the applied voltage of 20 kV. Below this concentration (3.5 and 4.0 wt%), a number of beads were

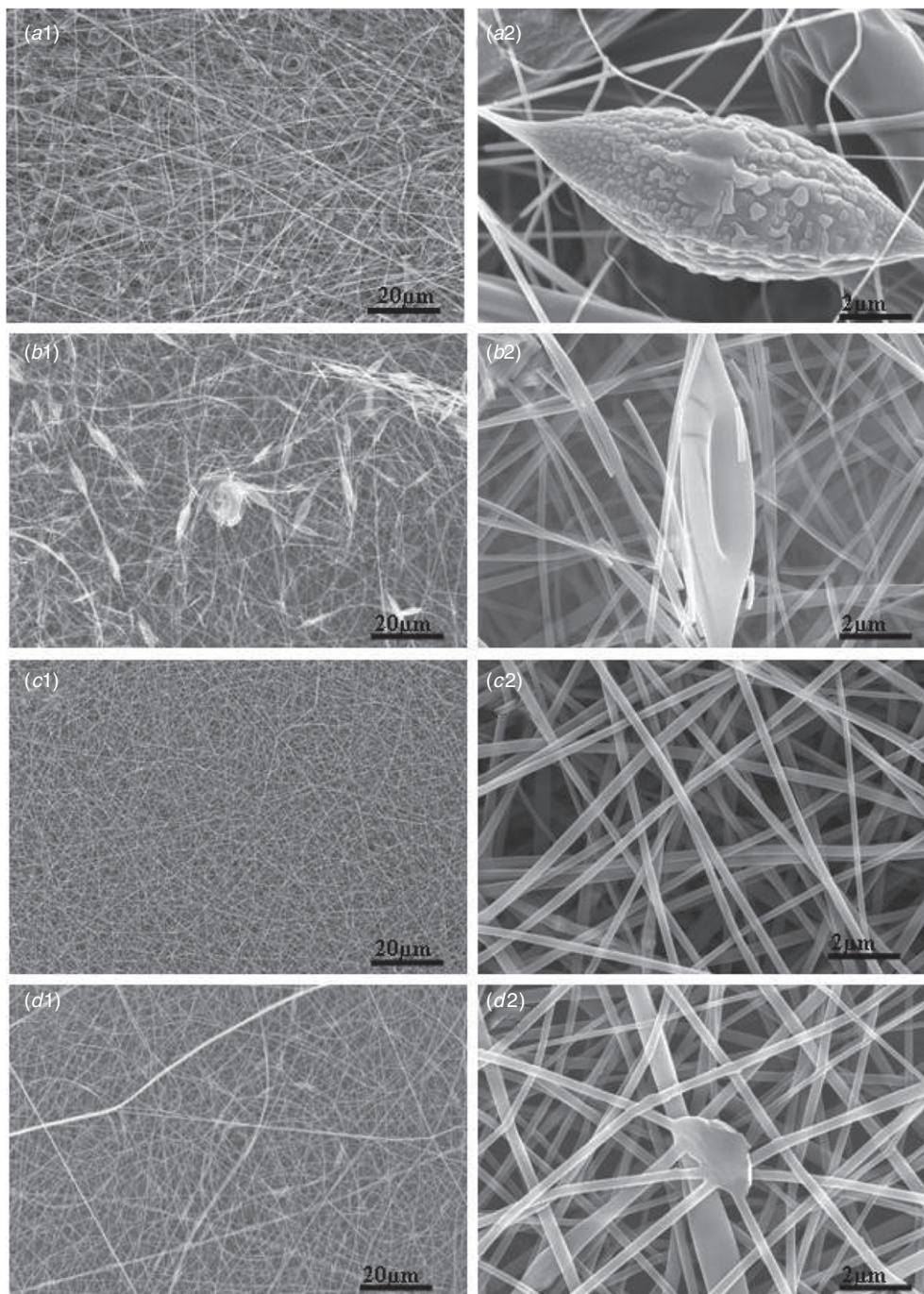


**Figure 1.** SEM microstructures of the electrospun magnetic biodegradable  $\text{Fe}_3\text{O}_4/\text{CS}/\text{PVA}$  nanofibrous membranes with polymer concentrations 3.5 wt% (*a1*, *a2*), 4.0 wt% (*b1*, *b2*), 4.5 wt% (*c1*, *c2*), and 5.0 wt% (*d1*, *d2*).

seen and the fibers were discontinuous (figures 1(*a1*), (*a2*) and (*b1*), (*b2*)). Heterogeneous nanofibers with spindle beads were achieved at polymer concentration of 5.0 wt% (figures 1(*d1*) and (*d2*)). The average diameter of nanofibers increased from  $280 \pm 26$  nm to  $310 \pm 76$  nm when the polymer concentration increased from 4.5 wt% to 5.0 wt%.

Fibers with a lot of spherical beads were fabricated under an applied voltage of 10 kV (figures 2(*a1*) and (*a2*)). When the applied voltage increased to 15 kV, the shape of the beads changed from sphere to spindle (figures 2(*b1*) and (*b2*)). When

the applied voltage increased to 20 kV, beads disappeared and the nanofibers possessed homogeneous surface morphology with an average diameter of  $280 \pm 32$  nm (figures 2(*c1*) and (*c2*)). Then, when the applied voltage further increased to 25 kV, heterogeneous nanofibers with a large size distribution of  $230 \pm 110$  nm were obtained (figures 2(*d1*) and (*d2*)).

All the  $\text{Fe}_3\text{O}_4/\text{CS}/\text{PVA}$  nanofibrous membranes with  $\text{Fe}_3\text{O}_4$  nanoparticles loading of 1, 3 and 5 wt% possess homogeneous, clear and continuous surface morphology (figures 3(*a1*)–(*c1*)). Fiber diameter distribution analysis

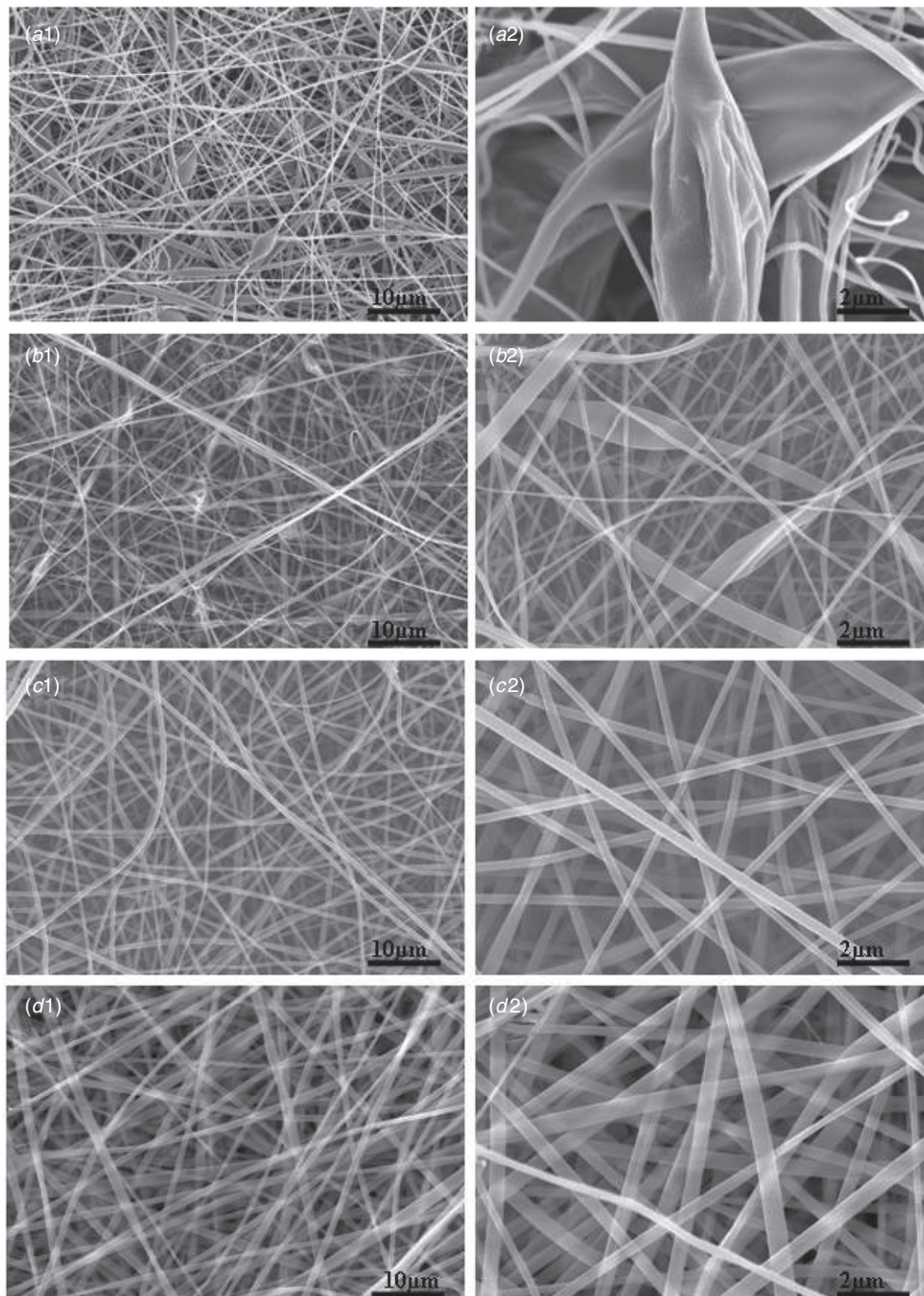


**Figure 2.** SEM microstructures of the electrospun magnetic biodegradable  $\text{Fe}_3\text{O}_4/\text{CS}/\text{PVA}$  nanofibrous membranes fabricated at the applied voltage of 10 kV(*a1, a2*), 15 kV (*b1, b2*), 20 kV (*c1, c2*), and 25 kV (*d1, d2*).

evaluated with ImageJ software was shown in figures 3(*a3*)–(*c3*). There was no significant difference between the diameters of the  $\text{Fe}_3\text{O}_4/\text{CS}/\text{PVA}$  nanofibrous membranes with  $\text{Fe}_3\text{O}_4$  nanoparticles loading of 1, 3 and 5 wt%, which were in the range of  $286 \pm 35$  nm,  $280 \pm 36$  nm, and  $290 \pm 43$  nm, respectively. TEM images showed that  $\text{Fe}_3\text{O}_4$  nanoparticles possess homogeneously spherical shape with diameter about 12–15 nm (figure 4). Islets of  $\text{Fe}_3\text{O}_4$  nanoparticles were evenly distributed in the nanofibrous membranes, and the number of

islets increased with the increase of the  $\text{Fe}_3\text{O}_4$  nanoparticles loading (figures 3(*a2*)–(*c2*)).

The characteristics of magnetic  $\text{Fe}_3\text{O}_4/\text{CS}/\text{PVA}$  nanofibrous membranes with homogeneous, clear and continuous surface morphology were summarized in table 1. It was clear that no significant difference were observed among the apparent densities ( $1.24$ – $1.28$   $\text{g cm}^{-3}$ ) and porosities (83.9–85.1%) of nanofibrous membranes at all level of  $\text{Fe}_3\text{O}_4$  nanoparticles loading, though the apparent densities of nanofibrous membranes slightly increased with the increase

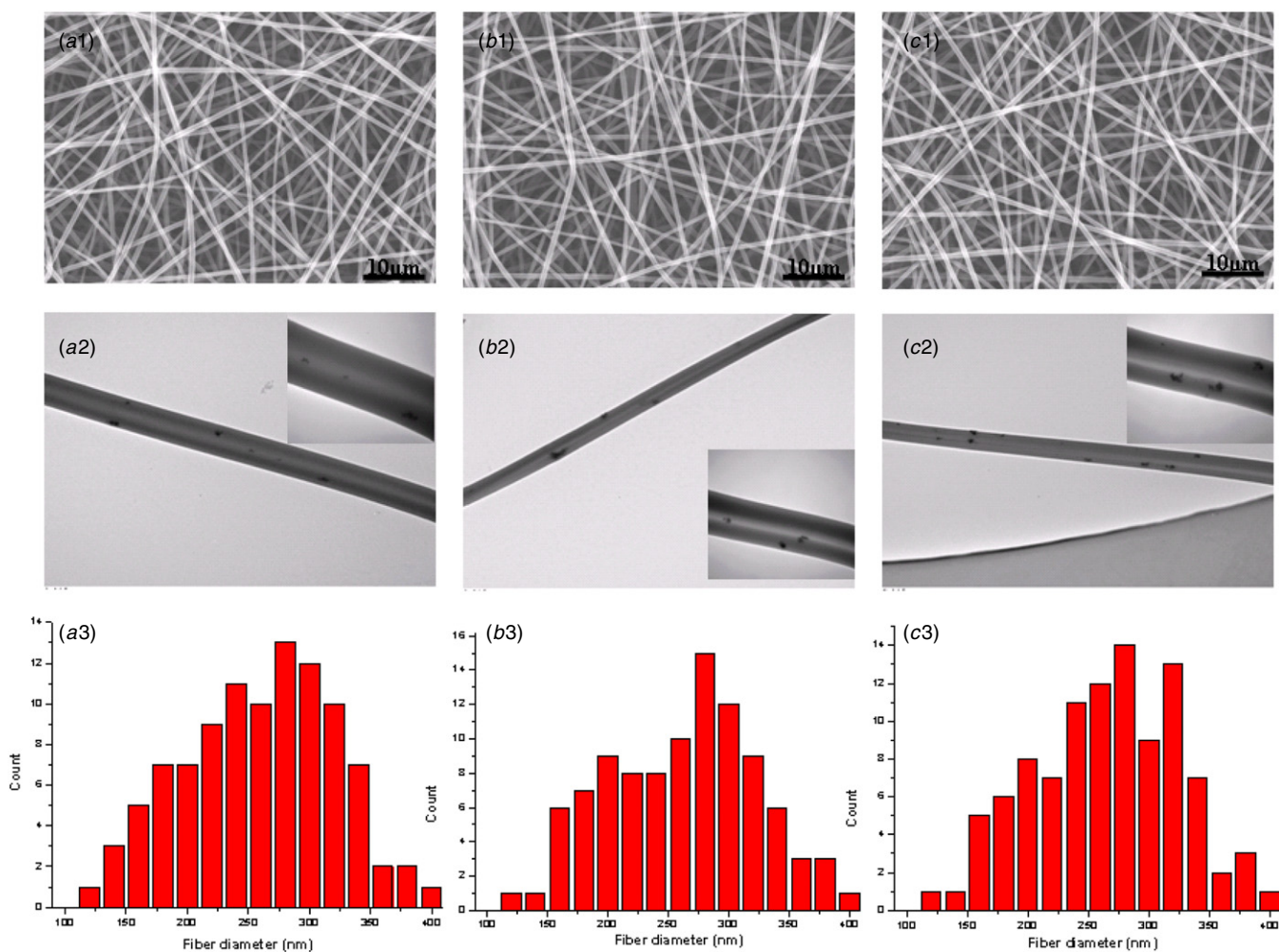


**Figure 3.** SEM microstructures, corresponding TEM images and fiber diameter distribution of Fe<sub>3</sub>O<sub>4</sub>/CS/PVA nanofibrous membranes with Fe<sub>3</sub>O<sub>4</sub> nanoparticles loading content of 1 wt% (a1, a2, a3), 3 wt% (b1, b2, b3) and 5 wt% (c1, c2, c3). Insets show the enlarged parts.

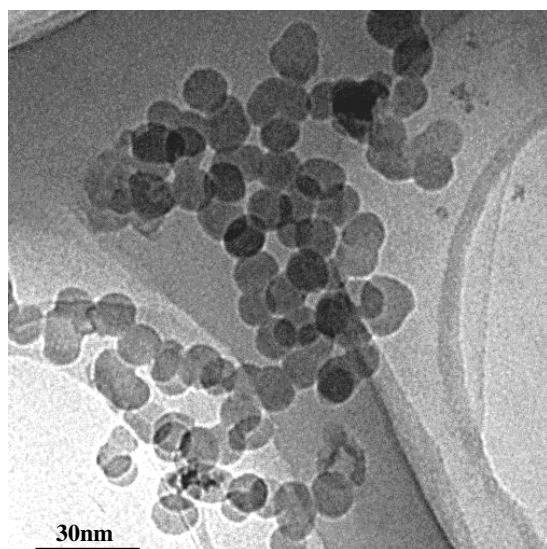


**Figure 4.** TEM images of Fe<sub>3</sub>O<sub>4</sub> nanoparticles synthesized by co-precipitation method and modified with sodium citrate.

**Table 1.** Porosity and apparent density of magnetic Fe<sub>3</sub>O<sub>4</sub>/CS/PVA nanofibrous membranes with different Fe<sub>3</sub>O<sub>4</sub> nanoparticles loading.

Samples	Apparent density (g cm <sup>-3</sup> )	Porosity (%)
0 wt% Fe <sub>3</sub> O <sub>4</sub> nanoparticles loading	1.24 ± 0.06	84.4 ± 5.36
1 wt% Fe <sub>3</sub> O <sub>4</sub> nanoparticles loading	1.25 ± 0.04	85.1 ± 7.13
3 wt% Fe <sub>3</sub> O <sub>4</sub> nanoparticles loading	1.27 ± 0.03	83.9 ± 6.59
5 wt% Fe <sub>3</sub> O <sub>4</sub> nanoparticles loading	1.28 ± 0.07	84.6 ± 8.34

of Fe<sub>3</sub>O<sub>4</sub> nanoparticles loading from 1.24 g cm<sup>-3</sup> (0 wt%), 1.25 g cm<sup>-3</sup> (1 wt%), 1.27 g cm<sup>-3</sup> (3 wt%), to 1.28 g cm<sup>-3</sup> (5 wt%).

### 3.2. Crystalline structure of the Fe<sub>3</sub>O<sub>4</sub>/CS/PVA nanofibrous membranes

To identify whether the Fe<sub>3</sub>O<sub>4</sub> nanoparticles were successfully incorporated into the nanofibrous membranes, and whether the electrospinning technique would change the crystalline structure of the components, XRD pattern of

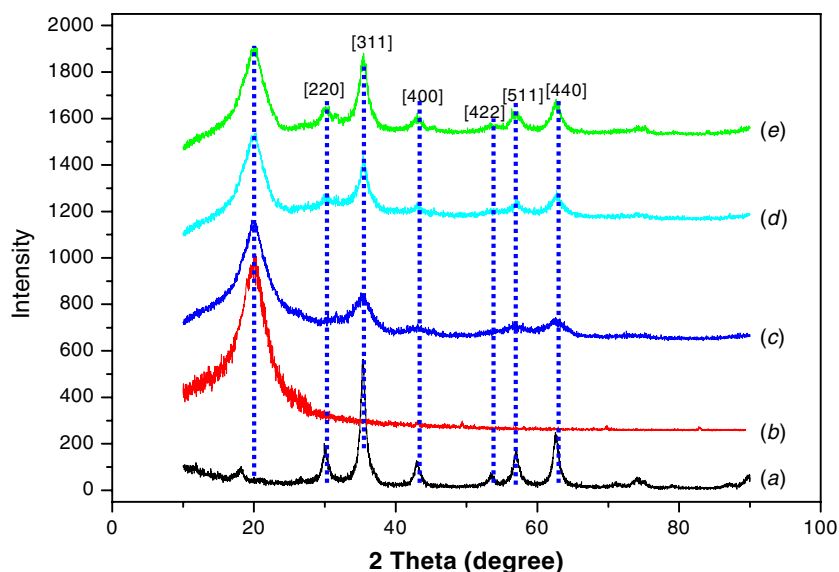


**Figure 5.** XRD patterns of  $\text{Fe}_3\text{O}_4$  nanoparticles (a),  $\text{Fe}_3\text{O}_4/\text{CS}/\text{PVA}$  nanofibrous membranes with  $\text{Fe}_3\text{O}_4$  nanoparticles loading of 0 wt% (b), 1 wt% (c), 3 wt% (d) and 5 wt% (e).

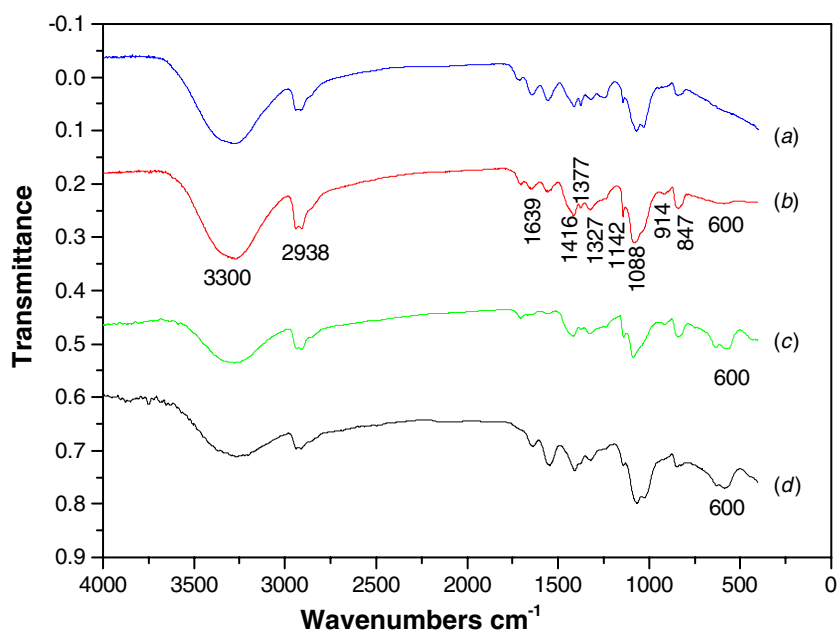


**Figure 6.** FT-IR spectra of  $\text{Fe}_3\text{O}_4/\text{CS}/\text{PVA}$  nanofibrous membranes with  $\text{Fe}_3\text{O}_4$  nanoparticles loading of 0 wt% (a), 1 wt% (b), 3 wt% (c) and 5 wt% (d).

the prepared nanofibrous membranes was examined. Figure 5 revealed that the  $\text{Fe}_3\text{O}_4/\text{CS}/\text{PVA}$  nanofibrous membranes possess one broad diffraction peak at  $2\theta$  values around  $20.4^\circ$  and six sharp diffraction peaks at  $2\theta$  values around  $30.0^\circ$ ,  $35.5^\circ$ ,  $43.1^\circ$ ,  $53.4^\circ$ ,  $57.0^\circ$  and  $63.0^\circ$  (figure 5(a)). The broad peak corresponds to the reflection peak of electrospun CS/PVA nanofibers (figure 5(b)). The other six sharp peaks, corresponding to the crystal planes of (2 2 0), (3 1 1), (4 0 0), (4 2 2), (5 1 1) and (4 4 0) of inverse cubic spinel structural  $\text{Fe}_3\text{O}_4$  (JCPDS 19-0629) (figure 5(c)).

### 3.3. FT-IR spectrum of the $\text{Fe}_3\text{O}_4/\text{CS}/\text{PVA}$ nanofibrous membranes

The FT-IR measurement of the composite was carried out in order to characterize the functional groups participated in the formation of magnetic  $\text{Fe}_3\text{O}_4/\text{CS}/\text{PVA}$  nanofibrous membranes. Figure 6 gave the FT-IR spectra of nanofibrous membranes with different  $\text{Fe}_3\text{O}_4$  nanoparticles loading. The CS exhibited characteristic broad bands around 914 and  $1142\text{ cm}^{-1}$  peaks assigned saccharine structure [38], characteristic peaks at  $1639\text{ cm}^{-1}$  were the absorption of  $-(\text{NH}_2)$  and  $-(\text{O}-\text{C}-\text{NH}_2)$  [39, 40], absorption features around

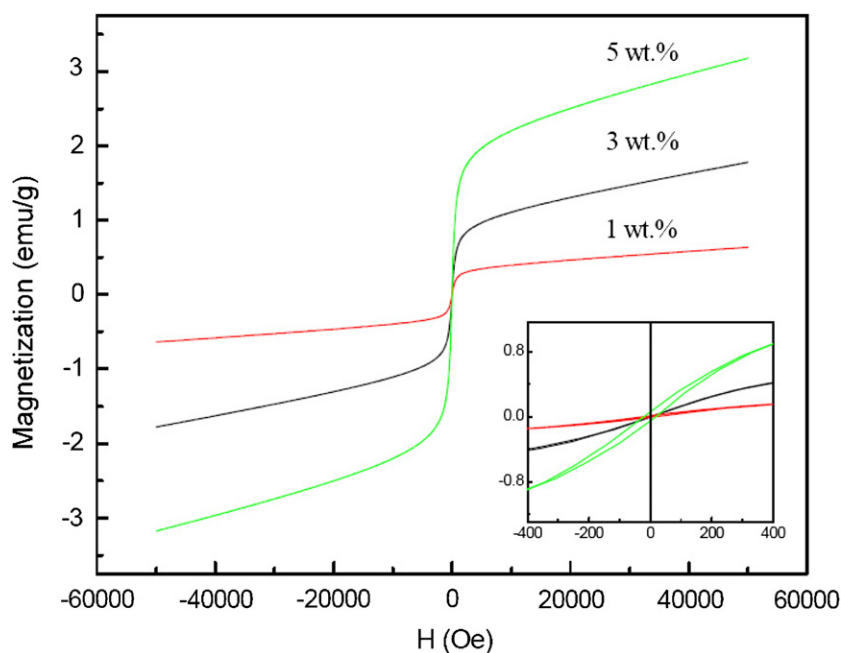


**Figure 7.** Hysteresis loops of the magnetic biodegradable  $\text{Fe}_3\text{O}_4/\text{CS}/\text{PVA}$  nanofibrous membranes with  $\text{Fe}_3\text{O}_4$  nanoparticles loading of 1%, 3% and 5 wt%.

**Table 2.** Mechanical properties' comparison of magnetic  $\text{Fe}_3\text{O}_4/\text{CS}/\text{PVA}$  nanofibrous membranes with different  $\text{Fe}_3\text{O}_4$  nanoparticles loading (the data are expressed as means  $\pm$  SD,  $n = 5$ ).

Samples	Ultimate tensile stress (MPa)	Ultimate tensile strain (%)	Young's modulus (MPa)
0 wt% $\text{Fe}_3\text{O}_4$ nanoparticles loading	$3.9 \pm 1.4$	$38.5 \pm 3.4$	$48.8 \pm 3.6$
1 wt% $\text{Fe}_3\text{O}_4$ nanoparticles loading	$3.9 \pm 1.3$	$38.1 \pm 2.3$	$52.0 \pm 3.9^*$
3 wt% $\text{Fe}_3\text{O}_4$ nanoparticles loading	$3.8 \pm 1.1$	$37.5 \pm 4.1$	$56.9 \pm 2.6^{**}$
5 wt% $\text{Fe}_3\text{O}_4$ nanoparticles loading	$3.6 \pm 1.3^*$	$36.6 \pm 3.7^*$	$58.4 \pm 3.7^{***}$

\*  $p < 0.05$ , \*\*  $p < 0.01$ , \*\*\*  $p < 0.001$ .

$3300 \text{ cm}^{-1}$  concerned with  $-(\text{OH})$  and  $-(\text{NH})$  stretching vibrations [41–43], and the peak at  $1377 \text{ cm}^{-1}$  was assigned to the  $-(\text{CH}_3)$  symmetrical deformation mode [38, 42]. A number of absorption peaks at 2938, 1416, 1327, 1088, and  $847 \text{ cm}^{-1}$  were attributed to the  $-(\text{CH}_2)$ ,  $-(\text{CH}-\text{OH})$ ,  $-(\text{CH}-\text{OH})$ ,  $-(\text{C}-\text{O})$  and  $-(\text{C}-\text{C})$  resonance of PVA, respectively [38, 42]. The characteristic absorption of  $-(\text{Fe}-\text{O})$  bond at  $600 \text{ cm}^{-1}$  indicated the present of  $\text{Fe}_3\text{O}_4$  in membranes [35], and this peak became more sharp in the membranes with higher  $\text{Fe}_3\text{O}_4$  loading.

### 3.4. Magnetic properties of the $\text{Fe}_3\text{O}_4/\text{CS}/\text{PVA}$ nanofibrous membranes

The magnetic properties of  $\text{Fe}_3\text{O}_4$  nanoparticles incorporated in nanofibers were explored. VSM examination showed that  $\text{Fe}_3\text{O}_4/\text{CS}/\text{PVA}$  nanofibrous membranes exhibited weak ferrimagnetic behaviors at a low applied magnetic field. The saturation magnetization ( $M_s$ ) of the nanofibrous membranes increased from  $0.67 \text{ emu g}^{-1}$  (1 wt%, figure 7(a)),  $1.79 \text{ emu g}^{-1}$  (3 wt%, figure 7(b)) to  $3.19 \text{ emu g}^{-1}$  (5 wt%, figure 7(c)), which basically kept a linear growth model

with the increase of  $\text{Fe}_3\text{O}_4$  nanoparticles loading.  $\text{Fe}_3\text{O}_4$  nanoparticles also showed ferrimagnetic behaviors and  $M_s$  of them was  $56.05 \text{ emu g}^{-1}$  (figure 8).

### 3.5. Tensile strength of the $\text{Fe}_3\text{O}_4/\text{CS}/\text{PVA}$ nanofibrous membranes

The change of the mechanical properties of the magnetic  $\text{Fe}_3\text{O}_4/\text{CS}/\text{PVA}$  nanofibrous membranes with different  $\text{Fe}_3\text{O}_4$  nanoparticles loading was investigated. The stress–strain curve shown in figure 9 and the detailed mechanical parameters listed in table 2 made it clear that the nanofibrous membranes resulting from  $\text{Fe}_3\text{O}_4$  nanoparticles loading of 0, 1 and 3 wt% exhibited no significant difference on the average ultimate tensile stress and ultimate strain. But the nanofibrous membranes with  $\text{Fe}_3\text{O}_4$  nanoparticles loading of 5 wt% possessed slightly reduced ultimate tensile stress and ultimate strain. Additionally, Young's modulus of membranes significantly enhanced with the increase of  $\text{Fe}_3\text{O}_4$  nanoparticles loading from 48.8 MPa (0 wt%), 52.0 MPa (1 wt%), 56.9 MPa (3 wt%), to 57.4 MPa (5 wt%).

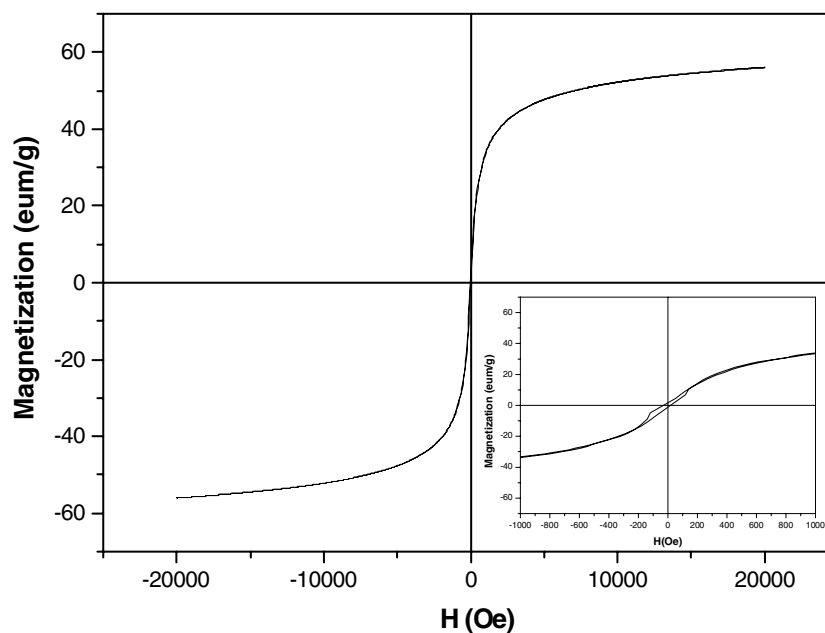


Figure 8. M–H hysteresis curves of  $\text{Fe}_3\text{O}_4$  nanoparticles synthesized by co-precipitation method and modified with sodium citrate.

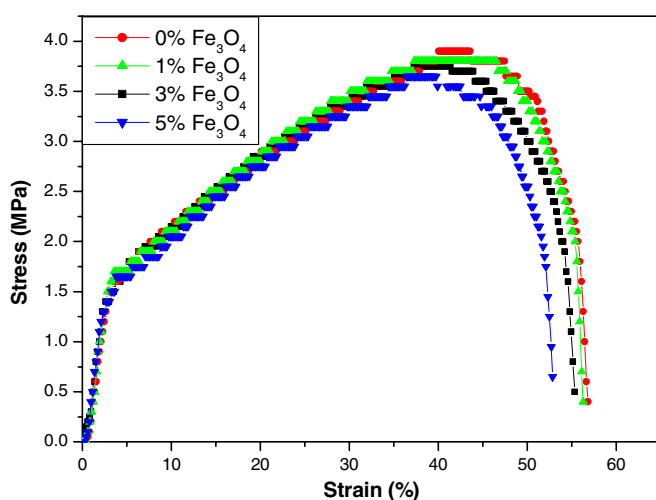


Figure 9. Typical stress–strain curves of the magnetic  $\text{Fe}_3\text{O}_4$ /CS/PVA nanofibrous membranes with different  $\text{Fe}_3\text{O}_4$  nanoparticles loading.

### 3.6. Cell growth dynamics of the $\text{Fe}_3\text{O}_4$ /CS/PVA nanofibrous membranes

SEM observation found that MG63 cells adhered and grew well on all nanofibrous membranes, and the cell proliferation increased with the increase of seeding time. Meanwhile, the nanofibrous membranes with higher  $\text{Fe}_3\text{O}_4$  nanoparticles loading showed better MG63 cell adhesion and proliferation (figures 10(a7)–(d7)). Especially on the nanofibrous membranes with  $\text{Fe}_3\text{O}_4$  nanofibers loading of 5 wt%, cells were confluent and appeared as a dense network throughout the membranes after seven days seeding (figure 10(d7)).

From MTT assay, time-dependent cell viability increase in all groups was observed (figure 11). On day one after cell seeding, no significant difference among the MG-63 cell viability on all kinds of substrates was observed ( $p > 0.05$ ). As culture time lapsed to three, five and seven days, cell proliferation on the nanofibrous membranes were significantly higher than that on TCPs ( $p < 0.05$ ). Totally, cell proliferation on all substrates increased with the increase of seeding time. Meanwhile, cell proliferation on nanofibrous membranes also exhibited an up-regulating trend along with the increase of  $\text{Fe}_3\text{O}_4$  nanoparticles loading. Statistical analysis showed that the nanofibrous membranes with 5 wt%  $\text{Fe}_3\text{O}_4$  nanoparticles loading possessed the highest cell viability ( $p < 0.05$ ), and the cell viability of the 3 wt%  $\text{Fe}_3\text{O}_4$  group was significantly higher than that of 0 and 1 wt%  $\text{Fe}_3\text{O}_4$  group at three, five and seven days experimental time point ( $p < 0.05$ ). No significant difference between the cell viability of 0 and 1 wt%  $\text{Fe}_3\text{O}_4$  group at all experimental time point was observed ( $p > 0.05$ ).

## 4. Discussion

In previous studies, nanofibrous scaffolds fabricated by electrospinning have been proven to be one kind of promising material for tissue regeneration [12–16]. Considering the literature evidences that magnetic nanoparticles could promote osteoinduction [10, 11] and electrospun nanofibrous scaffolds could mimic the natural extracellular matrix [12–16]. Biomimetic electrospun magnetic scaffolds may have potential application in bone tissue engineering. Some kinds of magnetic nanofibrous scaffolds have been achieved by the electrospinning technique [22–27]. However, in these studies, the electrospinning parameters, cell function and the potential of magnetic fibrous scaffolds in tissue engineering have not been clearly clarified. In this work, magnetic

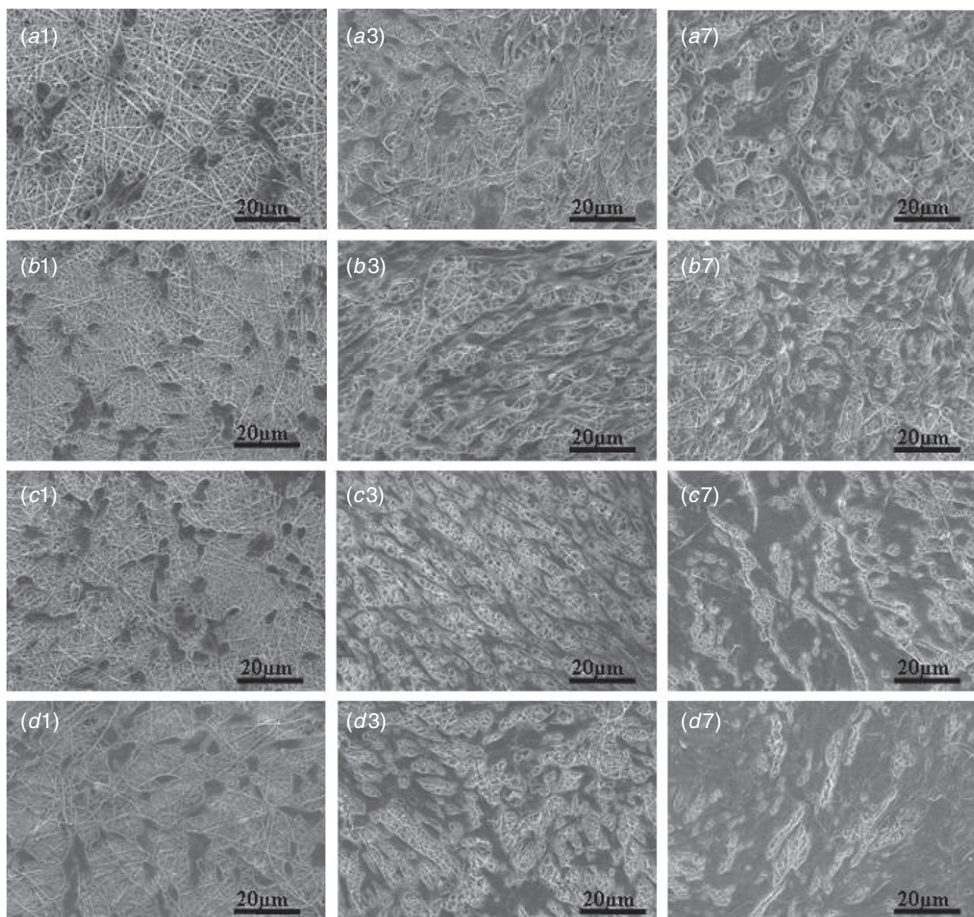


**Figure 10.** SEM images of MG-63 cells cultured *in vitro* for one day, three days and seven days on the Fe<sub>3</sub>O<sub>4</sub>/CS/PVA nanofibrous membranes with Fe<sub>3</sub>O<sub>4</sub> nanoparticles loading of 0 wt% (a1, a3, a7), 1 wt% (b1, b3, b7), 3 wt% (c1, c3, c7) and 5 wt% (d1, d3, d7).

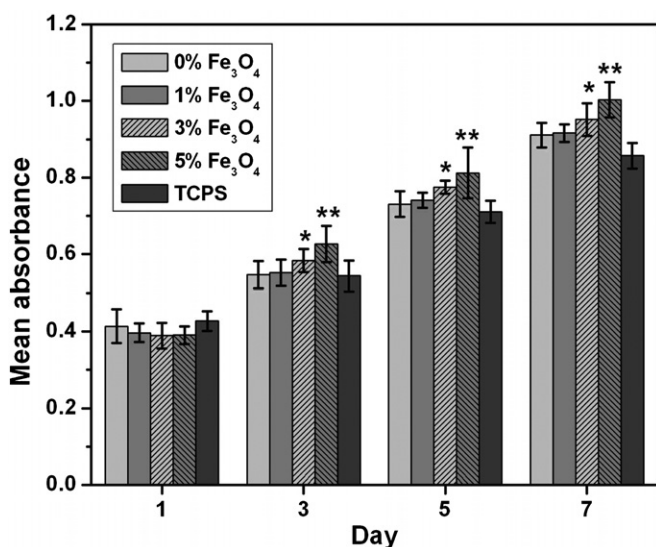


**Figure 11.** MTT assay of MG-63 on the magnetic biodegradable Fe<sub>3</sub>O<sub>4</sub>/CS/PVA nanofibrous membranes with Fe<sub>3</sub>O<sub>4</sub> nanoparticles loading content of 0%, 1%, 3% and 5 wt%; TCPs were used as control.

biodegradable Fe<sub>3</sub>O<sub>4</sub>/CS/PVA nanofibrous membranes were successfully fabricated by electrospinning process with the polymer concentration of 4.5 wt%, applied voltage of 20 kV and Fe<sub>3</sub>O<sub>4</sub> nanoparticles loading of lower than 5 wt%. Fe<sub>3</sub>O<sub>4</sub> nanoparticles loading of lower than 5 wt% was proven not to change the crystalline of the Fe<sub>3</sub>O<sub>4</sub>, CS, PVA and not to alter the functional groups participated in the formation of membranes significantly. The nanofibrous membranes were verified to show typical weak ferrimagnetic behaviors. Young’s modulus of membranes was gradually enhanced with the increase of Fe<sub>3</sub>O<sub>4</sub> nanoparticles loading, while ultimate tensile stress and ultimate strain were slightly reduced by Fe<sub>3</sub>O<sub>4</sub> nanoparticles loading of 5%. The promotion of MG63 cells growth dynamics suggested the magnetic biodegradable Fe<sub>3</sub>O<sub>4</sub>/CS/PVA nanofibrous membranes to be the promising scaffolds in bone regeneration.

In fabricating nanofibers by the electrospinning process, the balance among the electrostatic repulsion (determined by the applied voltage), surface tension and viscoelastic force (determined by the polymer concentration of solution) is reported to be the major factor to form and maintain a stable Taylor cone, leading to higher quality nanofibers [44, 45]. In present experiment, two key determining factors including applied voltage and polymer concentration were investigated respectively. With fixed applied voltage of 20 kV,

homogeneous and smooth surface were achieved only from solutions with the 4.5 wt% polymer concentration. Below this concentration (3.5 and 4.0 wt%), a number of beads were seen and the fiber was discontinuous. Heterogeneous nanofibers with spindle beads were achieved at polymer concentration of 5.0 wt%. This result was in agreement with what Deitzel *et al* [46] reported, that a mixture of fibers and droplets was produced for polymer concentration lower than 4 wt% during the electrospinning process. This is because the surface tension plays a dominating role in solution with lower polymer concentration of 3.5 and 4.0 wt% (lower viscous), the viscoelastic force is too weak to help stretch the fibers. When the polymer concentration increase to 4.5 wt% (more viscous), the surface tension is suppressed by electrostatic repulsion and viscoelastic force to form homogeneous nanofibers. However, heterogeneous nanofibers with a little spindle beads were achieved when the polymer concentration is further increased to 5.0 wt%, because the dominating viscoelastic force will break the force balance and lead to the instability of Taylor cone, which dedicate to the increase of heterogeneity of fibers [44, 46]. The average diameter of nanofibers increased with the polymer concentration increased from 4.5 wt% to 5 wt%, which is possibly attributed to that the fibers made from solution of higher polymer concentration own less solvent to evaporate during electrospinning process, which result in less reduction of mass loss [47].

It was demonstrated that the shape of nanofibers changed from beaded fibers to homogeneous and smooth ones gradually with the increase of applied voltage from 10, 15 to 20 kV, when the polymer concentration was preset at 4.5 wt%. The nanofibers obtained at voltage of 20 kV possessed the most homogeneous and smooth surface morphology. When the applied voltage increased to 25 kV, heterogeneous nanofibers were present again. The formation of beads may be ascribed to the instability of the jet at the spinning tip arising from lower voltage of 10 and 15 kV [4], while the relatively higher voltage (20 kV) could induce more charges to stretch the solution jet more easily and stably, which yield more uniform and smooth nanofibers [48–50]. The heterogeneity of nanofibers present at voltage of 25 kV is due to the fact that too high voltage will break the force balance and lead to the instability of Taylor cone, which was consequently dedicated to forming heterogeneous fiber.

Generally, the blend of inorganic particles may affect the morphology and size of electrospun nanofibrous membranes. Previous studies reported that PLGA, PLLA or collagen electrospun nanofibers with hydroxyapatite or tri-calcium phosphate particles showed random sizes and granule surface appearance due to serious particle agglomeration and insolubility of inorganic particles enveloped in the polymer matrix [51–53]. In present work, with polymer concentration of 4.5 wt% and applied voltage of 20 kV (according to above results), the Fe<sub>3</sub>O<sub>4</sub>/CS/PVA nanofibrous membranes were bead-free with a smooth surface at all levels of Fe<sub>3</sub>O<sub>4</sub> nanoparticles loading. This may due to that the Fe<sub>3</sub>O<sub>4</sub> nanoparticles loading of lower than 5 wt% did not change the surface tension and viscoelastic force of polymer solution greatly, and still kept the previous force balance to form

higher quality nanofibers. This presumption is further proven by the results that there is no significant difference between the diameters of the nanofibrous membranes at all levels of Fe<sub>3</sub>O<sub>4</sub> nanoparticles loading. Another reason is that the Fe<sub>3</sub>O<sub>4</sub> nanoparticles in our study were modified by sodium citrate to reduce the high surface energy and dipolar attraction, and the polymer solutions were mechanically stirred for 24 h and diffused with ultrasound for 2 h before electrospinning to keep Fe<sub>3</sub>O<sub>4</sub> nanoparticles evenly scattered in the polymer solutions. TEM observation verified that small islets composed of slight agglomeration of Fe<sub>3</sub>O<sub>4</sub> nanoparticles were well distributed inside the nanofibrous membranes. This phenomenon complies with most previous magnetic electrospun nanofibrous membranes [22–27]. Although almost all researchers have taken several measures to modify the Fe<sub>3</sub>O<sub>4</sub> nanoparticles, agglomeration still occurred. It is due to the fact that the magnetic attractive forces combined with inherently large surface energies (>100 dyn cm<sup>-1</sup>) of Fe<sub>3</sub>O<sub>4</sub> nanoparticles favor aggregation in fluids.

Porosity and apparent densities are important parameters to evaluate the utility of the fibrous materials for biomedical applications [21]. Table 1 showed that apparent densities of nanofibrous membranes slightly increased with the increase of Fe<sub>3</sub>O<sub>4</sub> nanoparticles loading, which is obviously due to the addition of Fe<sub>3</sub>O<sub>4</sub> nanoparticles. The porosity of the nanofibrous membranes with different Fe<sub>3</sub>O<sub>4</sub> nanoparticles loading was nearly the same value, about 84%. This is ascribed to the close similarities in the average fiber diameter and the morphology of the nanofibrous membranes [54]. The high porosity is beneficial to facilitate incorporating large amounts of tissue liquid for the supply of nutrients to the attached cells and nutrition/gas exchange [55, 56], which make magnetic Fe<sub>3</sub>O<sub>4</sub>/CS/PVA nanofibrous membranes ideal candidates for tissue engineering.

XRD pattern was carried out to characterize the phases of Fe<sub>3</sub>O<sub>4</sub>, CS and PVA in the electrospun nanofibrous membranes. Most electrospun magnetic fibrous scaffolds (Fe<sub>3</sub>O<sub>4</sub>/PVA nanofibers [22], Fe<sub>3</sub>O<sub>4</sub>/PVP nanofibers [23], FePt/PCL nanofibers [24], CoFe<sub>2</sub>O<sub>4</sub>/PAN nanofibers and CoFe<sub>2</sub>O<sub>4</sub>/carbon nanofibers [25]) were reported to maintain the crystalline of Fe<sub>3</sub>O<sub>4</sub> and other main polymer components, while Wang *et al* [24] reported the Fe<sub>3</sub>O<sub>4</sub>/C nanofibers owned different crystalline of the components, because the nanofibers were carbonized after electrospun. In this work, XRD pattern revealed that the Fe<sub>3</sub>O<sub>4</sub>/CS/PVA nanofibrous membranes possess one broad diffraction in accordance with the reflection peak of electrospun CS/PVA nanofibers and six sharp peaks consistent with the crystal planes of inverse cubic spinel structural Fe<sub>3</sub>O<sub>4</sub>. This result confirmed that the crystalline of Fe<sub>3</sub>O<sub>4</sub>, CS and PVA were maintained in the electrospun nanofibrous membranes. The stability of crystalline would definitely facilitate the electrospun nanofibrous membranes to express the biological effects of Fe<sub>3</sub>O<sub>4</sub>, CS and PVA.

FT-IR measurement was used for characterization and compositional analysis of nanofibrous membranes. Characteristic peaks attributed to resonance of CS/PVA were found in all groups. Compared to FT-IR spectra of 0 wt% Fe<sub>3</sub>O<sub>4</sub> group, specific absorption of the –(Fe–O) bond

indicated the present of Fe<sub>3</sub>O<sub>4</sub> in membranes with Fe<sub>3</sub>O<sub>4</sub> loading of 1, 3 and 5 wt%. Similar FT-IR spectra of membranes at all Fe<sub>3</sub>O<sub>4</sub> loading level demonstrate the Fe<sub>3</sub>O<sub>4</sub> loading up to 5 wt% did not change the functional groups of electrospun CS/PVA greatly. This result was supported by previous reports that addition of ZnO nanoparticles [43] and multi-walled carbon nanotubes (MWCNTs) [57] into CS/PVA films did not change the FT-IR spectra significantly. These phenomena favor the express of biological effects of Fe<sub>3</sub>O<sub>4</sub> and CS/PVA in tissue engineering.

The magnetic hysteresis loop showed that the Fe<sub>3</sub>O<sub>4</sub>/CS/PVA nanofibrous membranes exhibited typical weak ferrimagnetic behaviors. The saturation magnetization (Ms) of the Fe<sub>3</sub>O<sub>4</sub>/CS/PVA nanofibrous membranes at different level of Fe<sub>3</sub>O<sub>4</sub> loading were 0.67 em $\mu$  g<sup>-1</sup> (1 wt%), 1.79 em $\mu$ g<sup>-1</sup> (3 wt%) and 3.19 em $\mu$ g<sup>-1</sup> (5 wt%) respectively, while the Fe<sub>3</sub>O<sub>4</sub>/PVA nanofibers [22], Fe<sub>3</sub>O<sub>4</sub>/PVP nanofibers [23] and FePt/PCL nanofibers [26] also exhibited a Ms of lower than 5 em $\mu$ g<sup>-1</sup>, which are much lower than that of the Fe<sub>3</sub>O<sub>4</sub> nanoparticles (58 em $\mu$ g<sup>-1</sup>). This is attributed to the existence of nonmagnetic polymer components which encapsulate Fe<sub>3</sub>O<sub>4</sub> nanoparticles and affect the magnetization expression. Meanwhile, the Ms of the nanofibrous membranes were obviously enhanced by the increased Fe<sub>3</sub>O<sub>4</sub> nanoparticles loading and displayed a dose-dependent manner. This phenomenon suggests a possibility of regulating the magnetic properties of electrospun nanofibrous membranes by controlling the loading of Fe<sub>3</sub>O<sub>4</sub> nanoparticles.

The mechanical property of a tissue engineering scaffold is very important, as it needs to provide an initial biomechanical profile for the cells before new tissue can be formed. Similar stress-strain curve shapes of the magnetic Fe<sub>3</sub>O<sub>4</sub>/CS/PVA nanofibrous membranes with different Fe<sub>3</sub>O<sub>4</sub> nanoparticles loading demonstrated that the mechanical properties of nanofibrous membranes were not strongly affected by the incorporation of Fe<sub>3</sub>O<sub>4</sub> nanoparticles up to 5 wt%. The dependence of the mechanical parameters of membranes on Fe<sub>3</sub>O<sub>4</sub> nanoparticles loading is listed in more detail in table 2. The increase of Young's modulus of membranes with the increase of Fe<sub>3</sub>O<sub>4</sub> nanoparticles loading was supported by previous research about scaffolds containing inorganic nanoparticles [21, 58], which suggests a balance between biological effect and mechanical property of scaffolds related with the addition of nanoparticles should be taken into account, and that introducing inorganic nanoparticles could increase brittleness of scaffolds. Table 2 also made it clear that the membranes resulting from Fe<sub>3</sub>O<sub>4</sub> nanoparticles loading of 0%, 1% and 3% exhibit no significant difference on average ultimate tensile stress and ultimate strain, while they were significantly higher than those of 5 wt% Fe<sub>3</sub>O<sub>4</sub> group. This result is in accordance with some previous research. Prabhakaran *et al* [59] reported that the addition of HA decreased the tensile strength of electrospun PLLA. Vicentini *et al* [43] also found that the addition of ZnO nanoparticles significantly decreased the tensile strength of the CS/PVA films. This is because the nanoparticles distributed inside the fibers have no specific arrangement and therefore failed to

increase the ultimate tensile stress and ultimate strain of fibers. In addition, the presence of nanoparticles may probably reduce the effective diameter of fibers to support the external load. However, some other studies gave opposite results because of specific physical or chemical property of nanoparticles blended in scaffolds. Liao [57] attributed the enhanced tensile strength of the PVA/CS/MWCNTs nanofibrous mats to the alignment of MWCNTs in fibers. Young-Jin Kim ascribed the improved tensile strength of electrospun polyvinylidene fluoride/SiO<sub>2</sub> composite nanofiber membranes to that SiO<sub>2</sub> could act as temporary crosslinkers between polymer chains.

Cell adhesion onto scaffolds is the first fundamental step in bone regeneration, which will greatly influence the morphology and capacity of cell proliferation and differentiation [52]. Therefore, the cell adhesion and subsequent growth are essentially important markers to determine whether materials could be used as scaffolds in bone regeneration. In this work, MG63 cells were cultured on the Fe<sub>3</sub>O<sub>4</sub>/CS/PVA nanofibrous membranes to explore the cell growth dynamics. Compared to that on TCPs, cells cultured on nanofibrous membranes had a better growth on days three, five and seven, which is mainly due to the porous nanofibrous structures that facilitate the cell attachment and further proliferation. After seven days cell culture, both SEM observation and MTT assay showed that the cell adhesion and proliferation exhibited a tendency of increase with the increase of seeding time and the Fe<sub>3</sub>O<sub>4</sub> nanoparticles loading, suggesting that all substrates in this experiment have good biocompatibility and that Fe<sub>3</sub>O<sub>4</sub> nanoparticles contained in nanofibrous membranes can greatly improve the proliferation and growth of MG-63 cells. Similar results were obtained in several previous research about the osteoinductive effect of magnetic nanoparticles. Gu *et al* [10] indicated that, due to the tiny magnetic field provided by the magnetic nanoparticles, the integration of magnetic nanoparticles in CaP ceramics could promote the proliferation and differentiation of osteoblasts (Ros17/2.8 and MG63), and enhance the rhBMP-2 expression to accelerate the bone-like tissue formation. Meng *et al* [11] demonstrated addition of magnetic nanoparticles in hydroxyapatite nanoparticles (nHA)/poly (D,L-lactide) (PLA) composite nanofibrous films that induce a significantly higher proliferation rate and faster differentiation of osteoblast cells. The reason is probably that each magnetic nanoparticle could be regarded as a single magnetic domain, like a magnetic nanofield, once these magnetic nanoparticles were integrated in composite scaffolds, the micro-environments in the pores or on the surface of the scaffolds were composed of a great number of tiny magnetic fields, which would subsequently express osteoinductive effect of static magnetic fields. These positive results constitute the necessary prerequisites for further investigations into the potential of the magnetic scaffolds to direct osteogenesis, leading to subsequent bone tissue regeneration.

## 5. Conclusion

Homogeneous, smooth and continuous magnetic biodegradable Fe<sub>3</sub>O<sub>4</sub>/CS/PVA nanofibrous membranes

with porosity of 83.9–85.1% were successfully achieved by an electrospinning process with the polymer concentration of 4.5 wt% and applied voltage of 20 kV. It was proven that Fe<sub>3</sub>O<sub>4</sub> nanoparticles loading of lower than 5 wt% did not change the morphology of electrospun nanofibers. TEM showed islets of Fe<sub>3</sub>O<sub>4</sub> nanoparticles evenly distributed in the fibers. XRD data confirmed that the crystalline structure of Fe<sub>3</sub>O<sub>4</sub>, CS and PVA were maintained during electrospinning process. FT-IR demonstrated that the Fe<sub>3</sub>O<sub>4</sub> loading up to 5 wt% did not change the functional groups that participated in the formation of membranes greatly. VSM examination demonstrated these Fe<sub>3</sub>O<sub>4</sub>/CS/PVA nanofibrous membranes showing typical weak ferrimagnetic behaviors. Tensile examination exhibited that Young's modulus of membranes was gradually enhanced with the increase of Fe<sub>3</sub>O<sub>4</sub> nanoparticles loading, while ultimate tensile stress and ultimate strain were slightly reduced by Fe<sub>3</sub>O<sub>4</sub> nanoparticles loading of 5%. MTT assay and SEM observation exhibited promoted MG63 cells adhesion and proliferation on Fe<sub>3</sub>O<sub>4</sub>/CS/PVA nanofibrous membranes. The results of this work suggest that the magnetic biodegradable Fe<sub>3</sub>O<sub>4</sub>/CS/PVA nanofibrous membranes can be one of promising biomaterials for facilitation of osteogenesis. The increase of saturation magnetization, cell adhesion and proliferation along with the Fe<sub>3</sub>O<sub>4</sub> nanoparticles loading imply the possibility of further regulating cell function on magnetic electrospun nanofibrous membranes by control of the Fe<sub>3</sub>O<sub>4</sub> nanoparticles loading content.

## Acknowledgments

The authors acknowledge support from National Natural Science Foundation of China (no 51025205), the National High Technology Research and Development Program of China (2007AA03Z328766), International Science and Technology Cooperation Program (2007 DFA30690) and the Program of New Century Excellent Talents (NCET) of Universities in China.

## References

- [1] Sangsanoh P, Waleetorncheepsawat S, Suwanton O, Wutticharoenmongkol P, Weerananatanapan O and Chuenjitbuntaworn B 2007 *In vitro* biocompatibility of Schwann cells on surfaces of biocompatible polymeric electrospun fibrous and solution-cast film scaffolds *Biomacromolecules* **8** 1587–94
- [2] Schnell E, Klinkhammer K, Balzer S, Brook G, Klee D and Dalton P 2007 Guidance of glial cell. Migration and axonal growth on electrospun nanofibrous membranes of poly-epsilon-caprolactone and a collagen/ poly- epsilon-caprolactone blend *Biomaterials* **28** 3012–25
- [3] Oh S, Brammer K S, Li Y S J, Teng D, Engler A J and Chien S 2009 Stem cell fate dictated solely by altered nanotube dimension *Proc. Natl Acad. Sci. USA* **106** 2130–35
- [4] Yin Y J, Ye F, Cui J F, Zhang F J, Li X L and Yao K D 2003 Preparation and characterization of macroporous chitosan-gelatin beta-tricalcium phosphate composite scaffolds for bone tissue engineering *J. Biomed. Mater. Res. A* **67** 844–55
- [5] Arbab A S, Bashaw L A, Miller B R, Jordan E K, Lewis B K, Kalish H and Frank J A 2003 Characterization of biophysical and metabolic properties of cells labeled with superparamagnetic iron oxide nanoparticles and transfection agent for cellular MR imaging *Radiology* **229** 838–46
- [6] Wilhelm C, Billotey C, Roger J, Pons J N, Bacri J C and Gazeau F 2003 Intracellular uptake of anionic superparamagnetic nanoparticles as a function of their surface coating *Biomaterials* **24** 1001–11
- [7] Honda H, Shimizu K, Ito A, Arinobe M, Murase Y, Iwata Y, Narita Y, Kagami H and Ueda M 2007 Effective cell-seeding technique using magnetite nanoparticles and magnetic force onto decellularized blood vessels for vascular tissue engineering *J. Biosci. Bioeng.* **103** 472–8
- [8] Attaluri A, Ma R, Qiu Y, Li W and Zhu L 2011 Nanoparticle distribution and temperature elevations in prostatic tumours in mice during magnetic nanoparticle hyperthermia *Int. J. Hyperther.* **27** 491–502
- [9] Kamihira M, Akiyama H, Ito A and Kawabe Y 2010 Genetically engineered angiogenic cell sheets using magnetic force-based gene delivery and tissue fabrication techniques *Biomaterials* **31** 1251–9
- [10] Gu Z W, Wu Y, Jiang W, Wen X T, He B, Zeng X B and Wang G 2010 A novel calcium phosphate ceramic-magnetic nanoparticle composite as a potential bone substitute *Biomed. Mater.* **5** 015001
- [11] Meng J, Zhang Y, Qi X J, Kong H, Wang C Y, Xu Z, Xie S S, Gu N and Xu H Y 2010 Paramagnetic nanofibrous composite films enhance the osteogenic responses of pre-osteoblast cells *Nanoscale* **2** 2565–9
- [12] Venugopal J, Prabhakaran M P, Zhang Y Z, Low S, Choon A T and Ramakrishna S 2010 Biomimetic hydroxyapatite-containing composite nanofibrous substrates for bone tissue engineering *Phil. Trans. R. Soc. A* **368** 2065–81
- [13] Sill T J and von Recum H A 2008 Electrospinning: applications in drug delivery and tissue engineering *Biomaterials* **29** 1989–2006
- [14] Liao S, Li B J, Ma Z W, Wei H, Chan C and Ramakrishna S 2006 Biomimetic electrospun nanofibers for tissue regeneration *Biomed. Mater.* **1** 45–53
- [15] Yang X P, Wang B W, Cai Q, Zhang S and Deng X L 2011 The effect of poly (L-lactic acid) nanofiber orientation on osteogenic responses of human osteoblast-like MG63 cells *J. Mech. Behav. Biomed. Mater.* **4** 600–9
- [16] Zhang S, Huang Y Q, Yang X P, Mei F, Ma Q, Chen G Q, Ryu S and Deng X L 2009 Gelatin nanofibrous membrane fabricated by electrospinning of aqueous gelatin solution for guided tissue regeneration *J. Biomed. Mater. Res. A* **90** 671–9
- [17] Patel A C, Li S X, Wang C, Zhang W J and Wei Y 2007 Electrospinning of porous silica nanofibers containing silver nanoparticles for catalytic applications *Chem. Mater.* **19** 1231–38
- [18] Formo E, Lee E, Campbell D and Xia Y N 2008 Functionalization of electrospun TiO<sub>2</sub> nanofibers with Pt nanoparticles and nanowires for catalytic applications *Nano Lett.* **8** 668–72
- [19] Demir M M, Gulgun M A, Menceloglu Y Z, Erman B, Abramchuk S S and Makhaeva E E 2004 Palladium nanoparticles by electrospinning from poly(acrylonitrile-co-acrylic acid)-PdCl<sub>2</sub> solutions. Relations between preparation conditions, particle size, and catalytic activity *Macromolecules* **37** 1787–92
- [20] Wang C, Yan E Y, Huang Z H, Zhao Q and Xin Y 2007 Fabrication of highly photoluminescent TiO<sub>2</sub>/PPV hybrid nanoparticle-polymer fibers by electrospinning *Macromol. Rapid Commun.* **28** 205–09

- [21] Kim Y K, Y J, Ahn C H, Lee M B and Choi M S 2011 Characteristics of electrospun PVDF/SiO<sub>2</sub> composite nanofiber membranes as polymer electrolyte *Mater. Chem. Phys.* **127** 137–42
- [22] Wang S H, Wang C, Zhang B, Sun Z Y, Li Z Y and Jiang X K 2010 Preparation of Fe<sub>3</sub>O<sub>4</sub>/PVA nanofibers via combining *in situ* composite with electrospinning *Mater. Lett.* **64** 9–11
- [23] Wang H, Tang H, He J and Wang Q 2009 Fabrication of aligned ferrite nanofibers by magnetic-field-assisted electrospinning coupled with oxygen plasma treatment *Mater. Res. Bull.* **44** 1676–80
- [24] Wang L, Yu Y, Chen P C, Zhang D W and Chen C H 2008 Electrospinning synthesis of C/Fe<sub>3</sub>O<sub>4</sub> composite nanofibers and their application for high performance lithium-ion batteries *J. Power Sources* **183** 717–23
- [25] Mincheva R, Stoilova O, Penchev H, Ruskov T, Spirov I and Manolova N 2008 Synthesis of polymer-stabilized magnetic nanoparticles and fabrication of nanocomposite fibers thereof using electrospinning *Eur. Polym. J.* **44** 615–27
- [26] Song T, Zhang Y Z, Zhou T J, Lim C T, Ramakrishna S and Liu B 2005 Encapsulation of self-assembled FePt magnetic nanoparticles in PCL nanofibers by coaxial electrospinning *Chem. Phys. Lett.* **416** 317–22
- [27] Chen I H, Wang C C and Chen C Y 2010 Fabrication and characterization of magnetic cobalt ferrite/polyacrylonitrile and cobalt ferrite/carbon nanofibers by electrospinning *Carbon* **48** 604–11
- [28] Jia Y T, Gong J, Gu X H, Kim H Y, Dong J and Shen X Y 2011 Fabrication and characterization of poly (vinyl alcohol)/CS blend nano fibers produced by electrospinning method *Carbohydrate Res.* **346** 259–65
- [29] Liang D, Hsiao B S and Chu B 2007 Functional electrospun nanofibrous scaffolds for biomedical applications *Adv. Drug Deliv. Rev.* **59** 1392–412
- [30] Ignatova M, Manolova N and Rashkov I 2007 Novel antibacterial fibers of quaternized chitosan and poly(vinyl pyrrolidone) prepared by electrospinning *Eur. Polym. J.* **43** 1112–22
- [31] Mi F, Tan Y, Lang H and Sung H 2002 *In vivo* biocompatibility and degradability of a novel injectable-chitosan-based implant *Biomater.* **23** 181–91
- [32] Chuang W Y, Young T H, Yao C H and Chiu W Y 1999 Properties of the poly(vinyl alcohol)/chitosan blend and its effect on the culture of fibroblast *in vitro* *Biomaterials* **20** 1479–87
- [33] Jayakumar R, Shalumon K T, Binulal N S, Selvamurugan N, Nair S V, Menon D, Furuike T and Tamura H 2009 Electrospinning of carboxymethyl chitin/poly(vinyl alcohol) nanofibrous scaffolds for tissue engineering applications *Carbohydrate Polym.* **77** 863–9
- [34] Hwang T S, Son B, Yeom B Y, Song S H and Lee C S 2009 Antibacterial electrospun chitosan/Poly(vinyl alcohol) nanofibers containing silver nitrate and titanium dioxide *J. Appl. Polym. Sci.* **111** 2892–9
- [35] Yan W, Bing H, Xiaoyang H, Yuanhua L, Xinzhi W and Xuliang D 2011 Synthesis of Fe<sub>3</sub>O<sub>4</sub> Nanoparticles and their Magnetic Properties Rare Metal and Engineering accepted
- [36] Wang P, Zheng Q Z, Yang Y N and Cui D J 2006 The relationship between porosity and kinetics parameter of membrane formation in PSF ultrafiltration membrane *J. Membr. Sci.* **286** 7–11
- [37] Wataha J C, Craig R G and Hanks C T 1992 Precision of and new methods for testing *in vitro* alloy cytotoxicity *Dental Mater.* **8** 65–70
- [38] Zheng H, Du Y M, Yu J H, Huang R H and Zhang L 2001 Preparation and characterization of chitosan/poly(vinyl alcohol) blend fibers *J. Appl. Polym. Sci.* **80** 2558–65
- [39] Caixia X, Riyao C, Xi Z, Xiao C and Zhen C 2008 Preparation of PVA-GA-CS/ PVA-Fe-SA bipolar membrane and its application in electro-generation of 2,2-dimethyl-3-hydroxypropionic acid *J. Membr. Sci.* **307** 218–24
- [40] Mincheva R, Manolova N, Sabov R, Kjurkchiev G and Rashkov L 2004 Hydrogels from chitosan crosslinked with poly(ethylene glycol) diacid as bone regeneration materials *e-polymers* **058** 1–11
- [41] Boonsongrit Y, Mueller B W and Mitrevej A 2008 Characterization of drug–chitosan interaction by <sup>1</sup>H NMR, FTIR and isothermal titration calorimetry *Eur. J. Pharm. Biopharm.* **69** 388–95 2008
- [42] Shen X Y, Jia Y T, Gong J, Gu X H, Kim H Y and Dong J 2007 Fabrication and characterization of poly (vinyl alcohol)/chitosan blend nanofibers produced by electrospinning method *Carbohydrate Polym.* **67** 403–9
- [43] Vicentini D S, Smania A and Laranjeira M C M 2010 Chitosan/poly (vinyl alcohol) films containing ZnO nanoparticles and plasticizers *Mater. Sci. Eng. C-Mater. Biol. Appl.* **30** 503–8
- [44] Li D and Xia Y N 2004 Electrospinning of nanofibers: reinventing the wheel *Adv. Mater.* **16** 1151–70
- [45] Ji L W, Medford A J and Zhang X W 2009 Fabrication of carbon fibers with nanoporous morphologies from electrospun polyacrylonitrile/Poly(L-lactide) blends *J. Polym. Sci. B* **47** 493–503
- [46] Deitzel J M, Kleinmeyer J, Harris D and Tan N C B 2001 The effect of processing variables on the morphology of electrospun nanofibrous membranes and textiles *Polymer* **42** 261–72
- [47] Kim H, Choi Y, Kanuka N, Kinoshita H, Nishiyama T and Usami T 2009 Preparation of Pt-loaded TiO<sub>2</sub> nanofibers by electrospinning and their application for WGS reactions *Appl. Catal. A* **352** 265–70
- [48] Sui G, Yang X P, Mei F, Hu X Y, Chen G Q, Deng X L and Ryu S K 2007 Poly-L-lactic acid/hydroxyapatite hybrid membrane for bone tissue regeneration *J. Biomed. Mater. Res. A* **82** 445–54
- [49] Deng X L, Sui G, Zhao M L, Chen G Q and Yang X P 2007 Poly(L-lactic acid)/hydroxyapatite hybrid nanofibrous scaffolds prepared by electrospinning *J. Biomater. Sci.-Polym. Ed.* **18** 117–30
- [50] Sahoo S, Ang L T, Goh J C H and Toh S L 2010 Growth factor delivery through electrospun nanofibres in scaffolds for tissue engineering applications *J. Biomed. Mater. Res. A* **93** 1539–50
- [51] Yan N, Zhang X, Cai Q, Yang X, Zhou X, Wang B and Deng X 2011 The effects of lactidyl/glycolidyl ratio and molecular weight of poly(D,L-Lactide-co-Glycolide) on the tetracycline entrapment and release kinetics of drug-loaded nanofibers *J. Biomater. Sci. Polym. Ed.* **4** 21477461
- [52] Ma Z W, Kotaki M, Yong T, He W and Ramakrishna S 2005 Surface engineering of electrospun polyethylene terephthalate (PET) nanofibers towards development of a new material for blood vessel engineering *Biomaterials* **26** 2527–36
- [53] Liboff A R, Williams J T, Strong D M and Wistar J R 1984 Time-varying magnetic fields: effect on DNA synthesis *Science* **223** 818–20
- [54] Lee W J, Jung H R, Ju D H, Zhang X W and Kotek R 2009 Electrospun hydrophilic fumed silica/polyacrylonitrile nanofiber-based composite electrolyte membranes *Electrochimica Acta* **54** 3630–7
- [55] Lee J H, Park T G, Park H S, Lee D S, Lee Y K, Yoon S C and Nam J D 2003 Thermal and mechanical characteristics of poly(L-lactic acid) nanocomposite scaffold *Biomaterials* **24** 2773–8

- [56] Nam Y S and Park T G 1999 Porous biodegradable polymeric scaffolds prepared by thermally induced phase separation *J. Biomed. Mater. Res.* **47** 8–17
- [57] Zhang Y Z, Liao H L, H H, Qi R L, Shen M W, Cao X Y, Guo R and Shi X Y 2011 Improved cellular response on multiwalled carbon nanotube-incorporated electrospun polyvinyl alcohol/chitosan nanofibrous scaffolds *Colloids Surf. B* **84** 528–35
- [58] Kim G, Yeo M and Lee H 2011 Three-dimensional hierarchical composite scaffolds consisting of polycaprolactone, beta-tricalcium phosphate, and collagen nanofibers: fabrication, physical properties, and in vitro cell activity for bone tissue regeneration *Biomacromolecules* **12** 502–510
- [59] Prabhakaran M P, Venugopal J and Ramakrishna S 2009 Electrospun nanostructured scaffolds for bone tissue engineering *Acta Biomaterialia* **5** 2884–93